In Situ Near Crack Tip pH Measurements to Confirm Alkaline Crack Conditions Causing Crack Arrest in Cathodically Polarized AA5456-H116

Gabriella C. Montiel,[‡,] Saba Navabzadeh Esmaeely,[*] Gabriella Marino,[*] Jackson Pope,[*] Brandon Free,[*] Katrina E. Catledge,[*] Donald McAllister,[*] and Jenifer S. (Warner) Locke[*]*

In situ crack tip pH measurements for corrosion fatigue (CF) cracks in sensitized AA5456-H116 loaded under low loading frequencies show that cathodic polarization can arrest actively growing stress corrosion cracking (SCC) and CF cracks and produce a local alkaline crack tip pH. A method for measuring crack tip pH in situ was developed. For AA5456-H116 under a single level of high sensitization, CF experiments while loading in the Paris regime at a loading frequency of 0.1 Hz were conducted under freely corroding conditions and a cathodic polarization of −1.3 V_{SCE}. Results show that under freely corroding conditions the crack actively grows, and the crack tip pH is slightly acidic, while at −1.3 V_{SCE} an alkaline crack tip develops with a pH of 10 to 12. The findings of this study support the earlier published hypothesis that crack arrest of SCC and low loading frequency CF cracks is due to corrosion-induced blunting after the development of highly alkaline conditions that cause corrosion of the crack tip region blunting and halting the crack.

KEY WORDS: Al-Mg alloys, corrosion fatigue, cathodic corrosion-induced blunting

INTRODUCTION

Al-Mg alloys (AA5xxx series), which are used in marine environments due to their high strength-to-weight ratio, good weldability, low cost, and overall general corrosion resistance,[1-3] are strengthened through a combination of cold working and solid solution strengthening through the addition of 3.5 wt% to 5 wt% of Mg. However, due to the supersaturation of Mg, slightly elevated temperatures (~40°C) can facilitate the nucleation and growth of Al_3Mg_2 (aka β phase), which is anodic to the aluminum matrix, leaving these alloys susceptible to an electrochemical degradation process referred to as sensitization.[1,3-9] Sensitization is a process where an alloy becomes susceptible to intergranular corrosion (IGC) through the precipitation of a secondary phase with a distinctly different corrosion potential along grain boundaries. For AA5xxx alloys in the presence of a corrosive electrolyte, a microgalvanic couple exists between the β phase and near the grain boundary (GB) matrix leading to the dissolution of the anodic β-phase and severe IGC,[10-16] stress corrosion cracking (SCC),[17-27] and corrosion fatigue (CF).[6-7,19,28-32]

The severity of sensitization can be ascertained by ASTM G67 nitric acid mass lost tests (NAMLT),[33] where nitric acid preferentially dissolves the β phase and mass loss accumulates due to grain fallout when significant amounts of β phase have precipitates along the GBs. According to ASTM G67, NAMLT values from 1 mg/cm^2 to 15 mg/cm^2 are categorized as intergranular-resistant materials, values that fall between 15 mg/cm^2 and 25 mg/cm^2 have intermediate levels of sensitization and some susceptibility to IGC, and values that fall between 25 mg/cm^2 and 75 mg/cm^2 are heavily sensitized and most susceptible to IGC.[33]

Numerous studies have been conducted to understand the impact of sensitization on SCC and CF of the 5xxx series. The consensus is that crack growth rates increase with increasing sensitization[4,6-7,32,34] and with increasing applied anodic polarization.[2,21,35-36] Moreover, the thresholds below which SCC and CF cannot occur decrease with increasing sensitization.[7,26,29] Specifically for CF, the impact of sensitization, as measured by the difference in crack growth between unsensitized and sensitized microstructures, becomes more pronounced with decreasing fatigue loading frequency (f).[6-7,32,34]

The literature also reports ways to mitigate the effects of sensitization. One such way includes cathodic polarization, which has been reported to slow or completely stop cracking when polarizing below the breakdown potential for the β phase.[4-5,34-35] McMahon, et al., examined the potential dependence of SCC on highly sensitized AA5465-H116.[4,34] When studying a high level of sensitization within the range of potential of −0.6 V_{SCE} to 1.7 V_{SCE}, it was found that potentials at and below −1.0 V_{SCE} had low susceptibility to SCC.[4,34] In fact, when the potential was −1.3 V_{SCE} to 1.7 V_{SCE}, no SCC was observed, and evidence of corrosion-induced crack tip blunting was noted.[4,34] Finite element analysis to examine the stress fields near the crack

Submitted for publication: May 13, 2024. Revised and accepted: June 17, 2024. Preprint available online: June 19, 2024, https://doi.org/10.5006/4591.
‡ Corresponding author. E-mail: montiel.9@osu.edu.
* Department of Materials Science and Engineering, Fontana Corrosion Center, The Ohio State University, 2136 Fontana Labs, 140 W 19th Avenue, Columbus, Ohio 43210.

ISSN 0010-9312 (print), 1938-159X (online)

tip for the blunted geometries observed showed a significant decrease (more than 2-fold) in the maximum hydrostatic stress compared to a sharp crack tip noted in active SCC at higher potentials. It was surmised that the cathodic polarization facilitated crack tip conditions that caused corrosion-induced blunting, which decreased the stress field ahead of the crack to decrease the mechanical driving force for cracking to below the threshold required for SCC.[34] In studies conducted by Schrock examining CF of AA5456-H116 as a function of applied cathodic potential[35] and by Harris, et al., examining CF of sensitized AA5456-H116 at two cathodic potentials of −0.9 V_{SCE} and −1.3 V_{SCE} at a f of 5 Hz and a low f of 0.1 Hz,[5] the crack growth rate (da/dN) was found to be similar regardless of potential at f of 5 Hz while significant differences in da/dN as a function of applied potential arose at f of 0.1 Hz.[5,35] Specifically, applying a potential of −1.3 V_{SCE} stopped crack growth, resulting in a decrease in da/dN by over 1,000-fold compared to the higher potentials of between −0.8 V_{SCE} and −0.9 V_{SCE}.[5,34] The significant decrease in da/dN to complete crack arrest was attributed to corrosion-induced blunting at the crack tip.[5] It was postulated that the significant cathodic polarization increased the rate of cathodic reactions occurring within the crack to increase to such a degree that highly basic crack solutions developed.[5] Because Al alloys have passivity that is amphoteric, the low f allowed for passive film breakdown at the crack tip and within the wake causing significant corrosion under alkaline conditions to cause blunting of the crack tip. This did not occur under higher f loading because the shorter cycle time was able to maintain a sharp crack.[5] It also did not occur during anodic polarization, freely corroding conditions, or under minimal cathodic polarization as it is postulated that the typically slightly acidic crack conditions were not severe enough to cause corrosion anywhere except at the advancing crack tip itself.[5] To confirm crack tip blunting was occurring, tests were interrupted, and the crack tip was examined via optical microscopy to see that at f of 5 Hz, the crack tip remained sharp while at f of 0.1 Hz, the crack tip was blunted.[5] It was hypothesized that two factors govern the impact of corrosion-induced blunting at highly cathodic potentials for the 5xxx series alloys: (1) mechanical crack tip resharpening from the cyclic loading and (2) modification of the crack tip chemistry to a pH that needs to exceed around 8.6 to cause corrosion-induced blunting and override the crack tip resharpening.[5]

The objectives of this study are to utilize an in situ crack tip pH measurement system to confirm or refute the hypothesis for crack tip blunting in cathodically polarized AA5456-H116. The same lot of AA5456-H116 was studied and loaded using the same fatigue loading parameters as Harris, et al.,[5] while monitoring the pH at the crack tip flexible pH electrodes under cathodic polarization of −1.3 V_{SCE}.

EXPERIMENTAL METHODS

2.1 | Materials

AA5456-H116 plates with a nominal thickness of 6.35 cm manufactured by Aleris, Inc., were used in this study and previous relevant studies.[5-6,32] The composition and microstructural properties of this lot of material have been reported elsewhere.[32] Samples were sensitized using a lab oven at 100°C for 817 h, corresponding to an ASTM G67-18[33] NAMLT value of about 70 mg/cm^2. This level of sensitization was chosen because it is similar to the sensitization level from the previous study.[5,35]

[†] Trade name.

Compact tension (C[T]) specimens were machined with the load applied in the short transverse (S) direction (also known as the plate thickness direction) and the crack propagated in the longitudinal (L) direction (also known as the rolling direction). This loading orientation, conventionally referred to as S-L, was chosen as it was the orientation studied in the companion work[5-6,32,35] and it is the most susceptible as grain boundaries are aligned with the crack propagation direction. The nominal width and thickness of the C(T) specimens were 50.8 mm and 12.7 mm, respectively, with a notch length of 12.7 mm. Samples were machined such that crack growth occurred at the mid-thickness (t/2) of the original plate. To facilitate in situ measurement of crack tip pH, two boreholes were machined from the top surface of the C(T) sample terminating just below the fracture plane. The depth and diameter of the holes are 30.5 mm and 2.4 mm, respectively. The front edge (closest to the notch) of the first hole was located 5.5 mm away from the notch and the second hole was located 10.6 mm away from the notch. The specimen geometry can be seen in Figure 1.

2.2 | Corrosion Fatigue Crack Tip pH of 5456-H116

CF experiments on the C(T) specimens described above were executed in a polycarbonate environmental cell that held 3 L of 0.6 M NaCl solution. A total of 6 L of solution from an external reservoir was circulated throughout the duration of each experiment at a rate of 20 mL/min to avoid corrosion product buildup and significant solution chemistry changes within the environmental cell. Bulk pH measurements were taken before and after each experiment to ensure there were no significant changes in bulk pH. A Gamry 1010b[†] potentiostat with a three-electrode setup was utilized to monitor open-circuit potential and to apply potentials. The reference electrode was a saturated calomel electrode (SCE) and a platinum mesh encircling the sample served as the counter electrode. Fatigue loading was performed on either a servo-hydraulic or servo-electric load frame applying a sinusoidal load waveform. The C(T) specimens were loaded using clevis grips with ceramic-coated pins

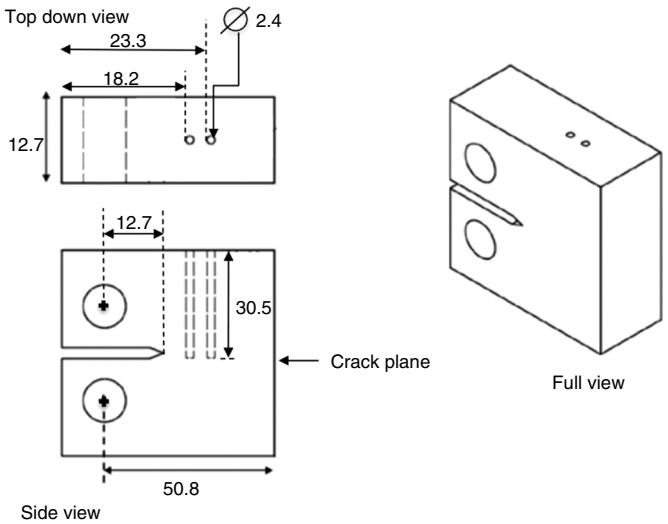

FIGURE 1. *Fracture mechanics samples used for CF testing while measuring crack tip pH, which were modified from the conventional C (T) specimen geometry by adding holes that terminate at the notch plane to accommodate pH electrodes for measurement of crack tip pH. All dimensions are in mm.*

to ensure electrical isolation from the load frame. The crack length was monitored continuously via the direct current potential drop (DCPD) method[36] with an applied current of 4 A. This current was reversed to minimize thermoelectric effects. The DCPD voltage was converted to crack length via Johnson's Equation.[36] All samples were fatigue precracked in load control, at room temperature in 0.6 M NaCl, at freely corroding conditions in accordance with ASTM E647[37] to a minimum of 1 mm from the notch using a stress intensity range ($\Delta K = K_{max} - K_{min}$) of 4.4 MPa$\sqrt{m}$, a stress ratio ($R = K_{min}/K_{max}$) of 0.43 or 0.78, and a f of 1 or 10 Hz. After precracking, each test was performed at a constant ΔK of 4.4 MPa$\sqrt{m}$, *f* of 0.1 Hz, and an R = 0.78.

To measure crack tip pH, esophageal pH electrodes from Microelectrodes, Inc. (part no. MI-508) were inserted in the boreholes shown in Figure 1. The reference electrode for these pH electrodes is external to facilitate a small diameter and flexibility by using a polymer sheath. Electrodes with incorporated reference electrodes to minimize the effects of IR drop have a glass sheath, which was found to break when the crack front entered the borehole. To ensure that an IR drop between the pH electrode and reference did not alter the measurement of crack tip pH when an external reference electrode was utilized, the pH and reference electrodes were placed in various position combinations (the reference either inside the first borehole and the active pH probe in the second borehole or reference placed outside the sample suspended in solution and active probes inside the boreholes). The reference electrode was also from Microelectrodes Inc. (part no. MI-402) and is comprised of an Ag-Ag/Cl internal reference electrode immersed in 3 M KCl. The experiment setup was done in such a way as to ensure the tip of the pH probe was located within the crack plane as best as possible. Calibration of pH electrodes was performed before and after each experiment by measuring the response, a voltage signal, in buffer solutions of pH 4, 7, and 10 to generate a calibration line to convert measured voltage into pH and ensure that the probe was not damaged during insertion, removal, or during the experiment. The pH values reported in this study were converted from the electrode voltage signal into pH values using the slope of the calibration curve collected in buffer solutions (averaging measured values taken before and after the test). It is important to note that select calibrations were conducted with a lower bound pH of 1 to ensure that calibration curve linearity was maintained down to acidic pH levels. An example calibration curve for these sets of experiments was shown in Figure 2.

After test termination, the solution was removed, and each sample was final fractured by ductile overload. Samples were cleaned after removal from the testing frame following ASTM G1.[23] Optical microscopy was utilized to measure the final crack length to correct crack length error within the DCPD reported crack length by using an assumption of linear accumulation of error. The error between the actual final and DCPD-reported crack lengths for these tests ranged from 5% to 13%. Once the DCPD crack length errors were corrected, these corrected crack lengths were used to calculate the actual applied ΔK from the applied load to confirm that loading was maintained within the valid bounds of the intended applied ΔK. Data collected between a ΔK of 4.2 MPa$\sqrt{m}$ and 5 MPa$\sqrt{m}$ were deemed acceptable, and data collected outside this range were rejected. This range was determined by examining the typical scatter for da/dN in previous work done on this lot of material.[32] The corrected crack length was also used to correlate pH measurements to the crack tip location. In the following figures, dashed lines will indicate the location of the borehole containing the pH measurement probe. Validation that the pH data were collected while the crack was within/near the borehole containing the probe or at some distance away in the wake was verified by using the corrected crack length and correlating this corrected crack length with the cycle count at which the pH data were registered. In all figures presenting pH data, these cycle counts where the crack was within the borehole are recorded with dashed lines.

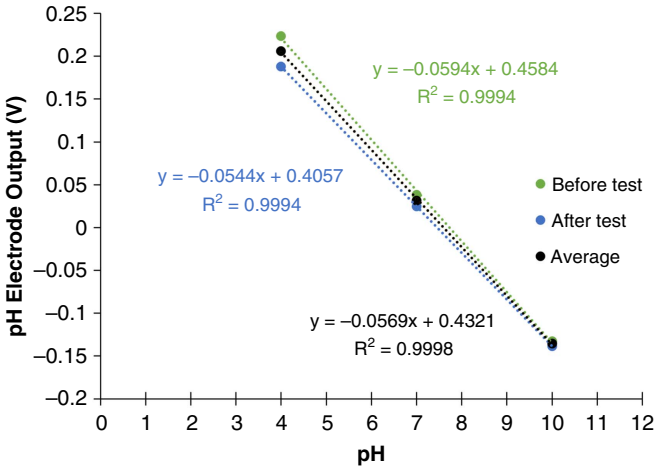

FIGURE 2. *pH calibration curves performed in buffer 4,7, and 10 done before test (green) and after test (blue), and the average line (black) is the line utilized to convert pH voltage signal to a pH value.*

It is important to note that most figures presented here do not have pH data plotted before the crack front enters the borehole. This is because the pH probe collects data the entire experiment, even prior to the crack front breaching the plane of the borehole. When the crack is at a crack length shorter than the distance to the borehole, the recorded voltage signal is representative of air as there is no electrolyte in the hole until the probe breaks the plane of the hole as the electrolyte level is always kept below the top surface plane of the sample. Typically, there is a large voltage shift, as will be explained in the *Results* section, when the probe contacts the solution. For the majority of results presented here, the data representative of the air signal is removed.

2.3 | Preliminary Studies Establishing Crack Tip pH Measurement Technique

Preliminary studies to ensure the addition of boreholes did not invalidate the K solution for the C(T) sample geometry were conducted on AA7075-T6 as the lab had pre-existing data against which to compare crack growth kinetics. The C(T) samples were machined in the S-L orientation. This set of C(T) samples had three boreholes machined in at locations of a/W of 0.45, 0.58, and 0.70, where W is 50.8 mm. These tests were to allow both validation of the K solution and to test the use of the flexible vs. glass sheath pH probes. All experimental setup procedures described above were used in these preliminary studies. Loading was conducted in 0.6 M NaCl with a constant ΔK of 6 MPa$\sqrt{m}$, R of 0.65, and f of 0.5 Hz; all of which were chosen to facilitate a constant crack growth rate across the entire valid a/W range. As the glass sheathed pH probes tended to fracture when the crack crossed the borehole plane, results comparing the two types of probes are not included in this paper.

RESULTS

3.1 | Preliminary Study on AA7075-T6 to Verify Validity of Procedure

Figure 3 shows the results of the preliminary study on AA7075-T6 loaded in 0.6M NaCl to ensure that addition of boreholes into the C(T) sample did not invalidate the K solution. Loading conditions were chosen to facilitate comparison with other data generated on a different program in the lab and were $\Delta K = 6\ MPa\sqrt{m}$, R = 0.65, and *f* = 0.5 Hz. Figure 3 plots the crack length versus cycle count for C(T) samples, with and without boreholes, with a linear regression fit for each test included to show both the da/dN and R^2 value for the fit for comparison. It can be seen that da/dN is constant at approximately 8.6×10^{-4} mm/cycle for all sample types regardless of the presence of boreholes. However, one sample with the boreholes (seen in orange in Figure 3) recorded a slightly lower da/dN at 6.4×10^{-4} mm/cycle, but this is within the allowable 2× scatter accepted by ASTM E647.[37] The R^2 values for each fit remain above 0.96, which establishes the stability of the experimental system over a wide range of a/W.

Another key element of this preliminary study was the utilization of the pH electrode to record pH during CF experiments. All experimental procedures were identical to those from the K solution validation experiments ($\Delta K = 6\ MPa\sqrt{m}$, R = 0.65, and *f* = 0.5 Hz). Before and after the experiment the pH electrode was calibrated using the buffer solution calibration method described above. Figure 4 shows the results from the CF testing with simultaneous recording of pH. Figure 4(a) shows the output voltages as function of cycle count, where the voltage abruptly increases at 26,000 cycles. Figure 4(b) shows the crack pH, converting from the output voltage to pH using the average calibration line, as a function of crack length. The position of the second probe hole, which contained the active pH electrode, is marked by the red dashed line with the "X". Once the crack tip breached the second borehole and exposed the electrode, the pH electrode recorded an acidic pH value of about 3. The bulk pH of the 0.6M NaCl was 6 to 7. As explained in the *Methods* section, the voltage readings collected before the crack front breaching the second borehole correspond to voltage readings in air, and not electrolyte, as the electrolyte level is always kept below the top surface plane of the sample. It is shown here for readers to understand the typical data output, but the voltage data corresponding to air will be removed in subsequent plots.

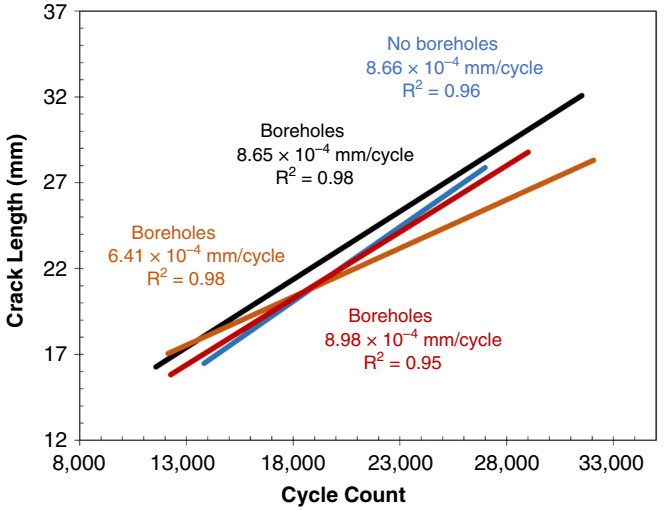

FIGURE 3. *Crack length as a function of cycle count for AA7075-T6 CT samples with and without probe holes. All tests were conducted under full immersion in 0.6 M NaCl under freely corroding conditions with an applied ΔK of 6 MPa√m, R of 0.65, and f of 0.5 Hz. A linear regression for each experimental data set is shown in the color corresponding to the data. The slope of the linear regression is equivalent to the crack growth rate. The raw data is not presented here solely the trendline for each data set is shown.*

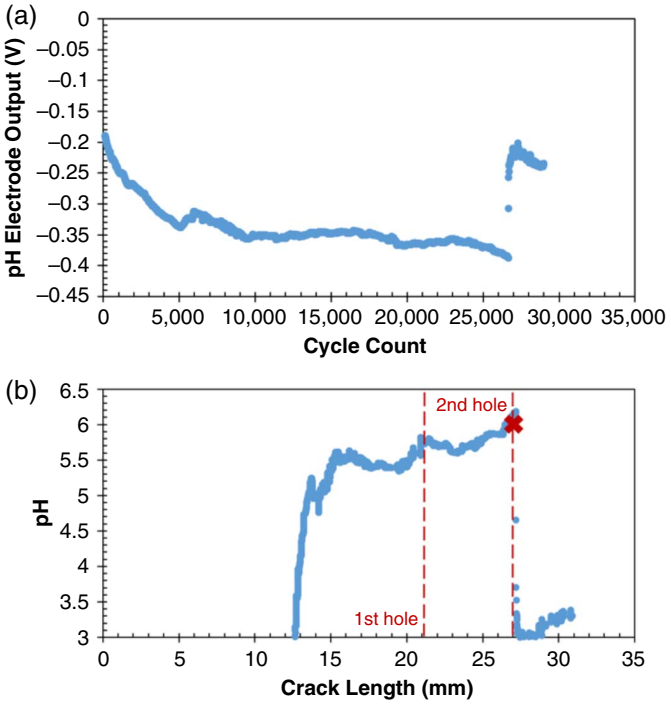

FIGURE 4. *Data from active crack tip pH measurement in AA7075-T6 under full immersion in 0.6 M NaCl under freely corroding conditions with an applied ΔK of 6 MPa√m, R of 0.65, and f of 0.5 Hz: (a) shows the raw data collected of output voltage vs. fatigue cycle count, (b) shows the pH calculated from the output voltage vs. crack length measured. The flexible pH microelectrode was placed in the second hole. The positions of the first and second hole are shown via the red dashed lines. The red X shows where the crack length corresponds to the crack plane reaching the second hole.*

The preliminary work shows that the modification of prior approaches[38] to measuring crack tip pH is effective to probe crack tip chemistry while actively loading a sample under fatigue loads in a load train. The use of flexible esophageal probes allows for increased success in experiments as probes with a glass sheath frequently broke when the fracture plane advanced to and through the probe hole. As a means of establishing that the pH measurement results in Figure 4 are reasonable and the experimental technique established here yields valid results, the results from a study by Cooper and Kelly[39-40] are used for comparison. Cooper and Kelly showed that the near crack tip electrolyte for AA7050-T6 loaded in 3.5% NaCl during SCC testing was between a pH of 2–3 and concentrated in $Al^{3+}$and Cl^{-}.[39-40] While modeling suggests that CF crack tip conditions may vary from SCC causing a pH closer to the bulk electrolyte, especially at high loading frequencies where the contribution of convective mixing becomes strong, very low loading frequencies, like those used here, may approach the SCC scenario.[41] The pH measured

here of about 3 is comparable to that measured by Cooper and Kelly,[39-40] which studied a similar Al-Cu-Zn-Mg alloy. Therefore, weight is given to the fact that the technique utilized in this study is valid.

3.2 | Measuring 5xxx Crack Tip pH as a Function of Polarization

As stated previously, to understand if a crack arrest of sensitized 5xxx aluminum alloys under severely cathodic polarization is caused by crack tip blunting from alkaline conditions causing corrosion broadly within the crack environment, CF testing was conducted at f of 0.1 Hz, with a ΔK of 4.4 MPa$\sqrt{m}$ and R of 0.78 under freely corroding and cathodically polarized conditions. Figure 5(a) shows crack length as a function of cycle count of an experiment with the pH reference electrode inserted in the first probe hole and the active pH measurement probe in the second probe hole. Figure 5(b) shows the active pH measurement in the second hole. The data plotted is that after voltage readings outside of the prior noise level were recorded (i.e., the electrode began reporting voltage signals significantly different than those recorded when the borehole was not exposed to solution). Examination of Figure 5, shows that under freely corroding conditions, denoted by the white regions in Figures 5(a) and (b), the crack is actively growing and when the cathodic polarization of −1.3 V_{SCE} is applied, the crack takes about 14 h to slow into arrest. This type of behavior is consistent with that reported in the prior work on this exact lot of AA5456-H116.[5,35]

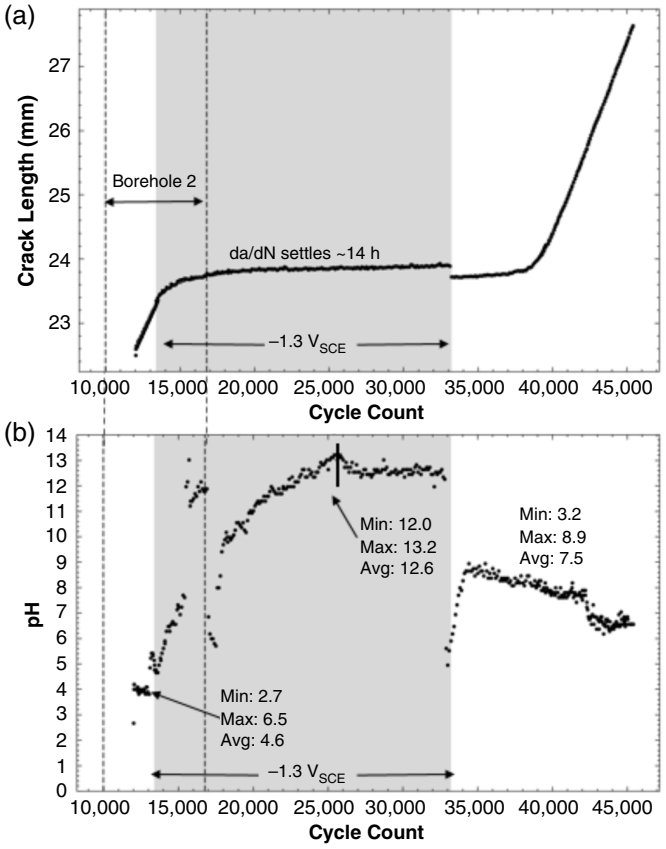

FIGURE 5. *Data for CF study of AA5456-H116 sensitized for 817 h at 100°C and loaded at a DK of 4.4 MPa$\sqrt{m}$, R of 0.78, and* f *of 0.1 Hz while fully immersed in 0.6 M NaCl where the reference electrode is placed within the first borehole. (a) Crack length as a function of cycle count. (b) Measured pH as a function of cycle count. The white background denotes data collected while freely corroding conditions were observed, and the gray background denotes when the cathodic polarization of −1.3 V_{SCE} was applied. The dashed lines indicate the location of the borehole in relation to the collected data. The borehole is 2.4 mm in diameter. To determine the location of the dashed lines, the known location of the hole was correlated with the corrected crack length data post-test to determine the fatigue loading cycle counts the crack was within the borehole.*

To understand how crack tip pH changed during these changes in potential, freely corroding conditions were maintained until after the active pH electrode became exposed to solution and began recording a signal outside of the prior level representative of air. As shown by the dashed lines, this occurred about midway through the borehole. While freely corroding with active propagation of the crack, the pH was measured for 3.5 h and an average pH of 4.6 was recorded.

Once the pH in the freely corroding portion of the test was established, the cathodic potential of −1.3 V_{SCE} was applied (indicated by the gray background in Figures 5[a] and [b]). This potential was held for a total time of 55 h. Over the first 14 h, da/dN slowed until the crack arrested during which time the crack grew 0.8 mm with the crack tip near the end of the borehole. In Figure 5(b), it can be seen that as the crack slows during these 14 h, the crack tip pH begins to rise. At 6 h into the polarization at −1.3 V_{SCE}, a substantial jump in pH occurs where the pH reaches a high of 13 before falling to a low of 5.5 and beginning to climb again. This period of scatter occurs over a 30 min period and correlates to a corrected crack length at the end of the second borehole. While it is not certain why this quick fluctuating shift in pH occurs, it may be that as the crack front broke through the end of the borehole increased mixing occurred with the bulk solution although this was not seen in the repeat test. The crack propagation rate does not show any anomalous trend during this time and continued to slow to arrest. After this anomalous pH behavior, the pH increased while the crack was arrested until eventually reaching a plateau at 32 h from the start of the polarization maintaining an average pH of 12.6 ± 0.6 until releasing the potential hold and returning to freely corroding conditions, as seen in Figure 5(b).

Upon releasing the applied potential and allowing freely corroding conditions to resume, indicated by the white background on the right-hand side of Figures 5(a) and (b), the crack remained arrested for about 16 h before growth resumed. During this second freely corroding segment, there is an initial steep drop in pH to 3.2 at the moment the potentiostatic hold is ended and a subsequent increase in pH to a max pH of 8.9 before stabilizing at an average near-neutral pH of 7.5 after 2 h. The pH later drops toward 6, but the crack tip had advanced past the hole at this time and the crack wake is being measured.

Figure 6 shows an optical micrograph of the fracture surface post-test for the experiment in Figure 5. The cathodic polarization creates a visible line on the fracture surface, which was similar to that seen in the prior publication.[5,35] This allows for demarcation of the location of crack arrest and provides confirmation that the crack tip had breached the second probe hole containing the active pH probe and was recording the near crack tip pH during the measurements reported in Figure 5(b).

Two other CF experiments were conducted at 0.1 Hz with these same loading conditions. The results of all are shown in Table 1. As one experiment, the one not shown in detail here is identical to the one discussed in Figure 5, the detailed data is not shown; only the pH measurement results are presented, which

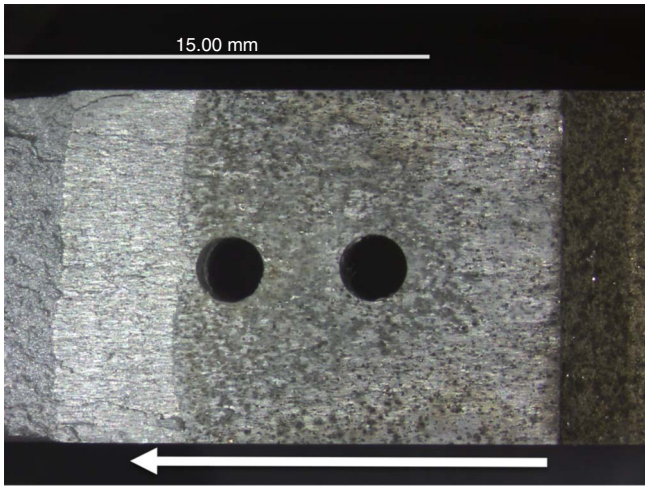

FIGURE 6. *Optical micrograph of the fracture surface post-test for the experiment in Figure 5.*

Table 1. *Summary of Experiments for AA5456-H116 Sensitized for 817 h at 100°C and Loaded at a DK of 4.4 MPa$\sqrt{m}$, R of 0.78, and f of 0.1 Hz While Fully Immersed in 0.6 M NaCl*[(A)]

Potential	Location of pH Reference Electrode	pH	Sample
Freely corroding	1st borehole	4.6	Figure 5
Freely corroding	Adjacent to sample	2.8	Full data not presented
−1.3 V_{SCE}	1st borehole	12.6	Figure 5
−1.3 V_{SCE}	Adjacent to sample	13.0	Full data not presented
−1.3 V_{SCE}	Adjacent to sample	12.0	Figure 7
−1.3 V_{SCE}	Away from sample	12.0	Figure 7
−1.3 V_{SCE}	Adjacent to sample	12.1	Figure 7

[(A)] The pH values listed below are average values taken from experiments.

are comparable to those in Figure 5 with an average freely corroding pH of 2.8 and a pH of 13.0 for the 1.3 V_{SCE} polarization.

Figure 7 shows the details of an experiment where the reference electrode was moved to different locations within the environmental containment cell to validate that solution IR drop was not creating a significant error in the crack tip pH measurements. For this experiment, the same loading condition of a ΔK of 4.4 MPa$\sqrt{m}$ and R of 0.78 was observed with freely corroding and the −1.3 V_{SCE} polarization used. For this test, active pH probes were located within the first and second boreholes. The probe located in the first borehole was damaged during testing; therefore, the data is not presented here. Figure 7(a) shows crack length as a function of cycle count for this experiment where the reference electrode is located outside the sample at varying distances from the sample surface. The crack growth trend is identical to that seen in Figure 5 with active crack propagation during the freely corroding portion of

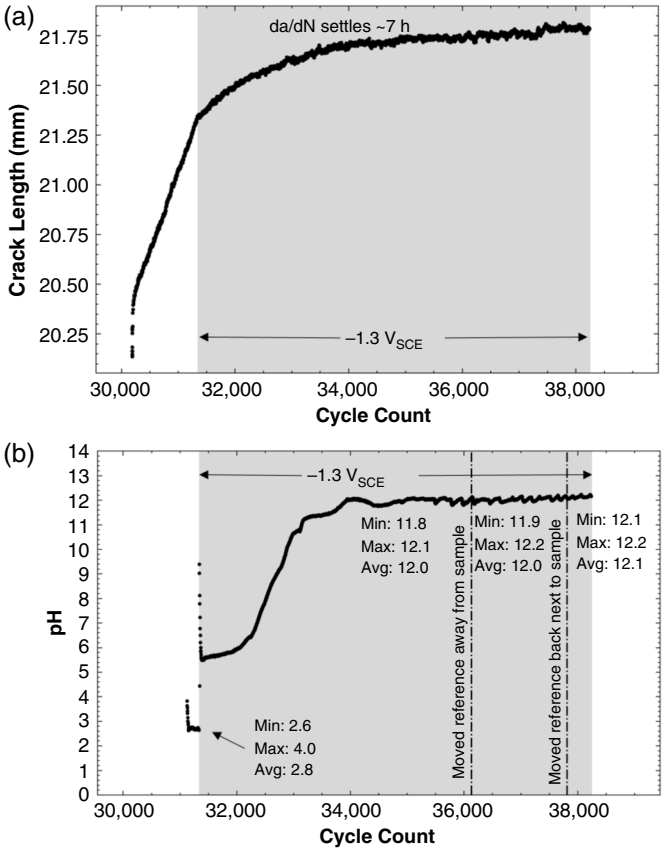

FIGURE 7. *Data for CF study of AA5456-H116 sensitized for 817 h at 100°C and loaded at a DK of 4.4 MPa$\sqrt{m}$, R of 0.78, and f of 0.1 Hz while fully immersed in 0.6 M NaCl where the reference electrode is placed at various locations outside of the sample. (a) Crack length as a function of cycle count. (b) Measured pH as a function of cycle count. The white background denotes data collected while freely corroding conditions were observed, and the gray background denotes when the cathodic polarization of −1.3 V_{SCE} was applied. The dashed/dotted lines in (b) indicate when the reference probe was moved and to where. All data shown here was collected within the borehole.*

testing (shown in the white background region); and upon application of −1.3 V_{SCE}, the crack slows for about 7 h before arresting (the crack grew 0.4 mm during this time). As shown in Figure 7(b), once the crack breached the second hole, the initial pH of the actively growing crack at the freely corroding potential was measured for 3 h with an average pH of 2.8 before applying the cathodic polarization of −1.3 V_{SCE} for a total of 19 h. During this segment of testing, the reference electrode was placed just outside of the sample next to the sample surface near the boreholes. Upon application of the cathodic potential, the crack tip pH quickly spiked to a value between 9 and 10 and then quickly went down to approximately 5.5 before slowing rising and eventually plateauing at an average pH of 12. The reference electrode was moved away from the sample surface toward the edge of the environmental cell after 13 h of applying −1.3 V_{SCE}. This is a distance greater than 60 mm from the sample surface. When the pH reference electrode was moved far away from the sample (denoted in Figure 7[b]), the pH of 12.0 was maintained. For the final hour of the experiment, 5 h after moving the reference electrode away from the sample surface, the pH reference electrode was moved back near

the sample surface. Again, the measured pH measured remained steady. The test was terminated while the crack tip was still within the borehole.

DISCUSSION

The results of this study lend supporting evidence to the earlier published hypothesis by Harris, Dubas, Schrock, Locke, and Burns that crack arrest of low loading frequency CF cracks is due to corrosion-induced blunting after the development of highly alkaline conditions that cause corrosion of the crack tip region to blunt and halting the crack.[5] The results of this study show that the low loading frequency CF crack tip pH under freely corroding conditions is between 2 and 5, which is acidic to the bulk pH, and under severe cathodic polarizations sufficient to halt a growing crack, a crack tip pH of 12 to 13 develops. These findings also support the earlier SCC work of McMahon, et al., which found a similar crack arrest phenomenon in SCC under cathodic polarizations of −1.3 V_{SCE} to −1.7 V_{SCE}.[34] The results of the current work also support the idea that active growth of CF in 5xxx Al alloys occurs when crack tip conditions are acidic.

Acidic crack tip conditions during SCC at freely corroding or under anodic polarization of other Al alloys have been noted in the past.[38-40,42] In a study performed by Cooper and Kelly, a similar method with pH microelectrodes was utilized to measure crack tip SCC in AA7050 in wedge open-loaded samples with glass-sheathed electrodes.[38] Cooper and Kelly found that at freely corroding conditions the pH was acidic at a pH of 3.5 when loading under immersion aqueous sodium chloride solutions.[38] Additionally, Nguyen, et al., found using capillary electrophoresis (CE) that SCC crack tips in 7075-T651 polarized to the corrosion potential under immersion in aqueous sodium chloride solution at a pH of 3.4.[42] These values are within the range of the pH measured here for 5456-H116 under freely corroding condition under CF conditions at an f of 0.1 Hz and ΔK of 4.4 MPa$\sqrt{m}$.

The cathodically polarized near crack tip pH measured in this study of 12 to 13 is also similar to that found in other Al alloys.[42] In the same study conducted by Nguyen, et al., on AA7075-T651 under SCC loading conditions in aqueous sodium chloride solutions, cathodic potentials of −1.065 V_{SHE} yielded a basic crack tip of 12 and SCC was mitigated.[42] This is again consistent with the crack tip conditions found in this study suggesting that CF experiments at a f of 0.1 Hz produce similar crack tip chemistries as SCC meaning that (1) the role of convective mixing is small compared to ion migration and diffusion and (2) that sensitized 5xxx and 7xxx Al alloys have similar crack tip chemistries.

The findings of this work provide useful information toward service considerations when using protection methods that employ cathodic polarization. Confirmation that corrosion-induced crack blunting is the most likely cause of the crack arrest observed in fracture mechanics lab testing when under large cathodic polarizations is important as it can inform on when service conditions can facilitate protection from metal-rich printers and not. Specifically, the prior CF study showed that high loading frequency did not produce crack arrest under similar cathodic polarizations.[5] While this study did not probe the crack tip conditions at higher f, the lack of crack arrest at higher f may be due to (1) the increased role of convective mixing mitigating the occluded alkaline pH and maintaining more bulk like pH conditions in the crack or (2) the ability of the mechanical loading conditions to maintain a sharp crack tip through mechanical resharpening. Should service conditions facilitate increased mixing of a crack environment with a less alkaline environment or loading events that allow for mechanical resharpening to occur crack growth could occur. As such, it is important to understand the limitations of cathodic protection systems on mitigation of SCC and CF of sensitized 5xxx Al alloys.

CONCLUSIONS

The results here show an effective and repeatable method for measuring crack tip pH and produce evidence to support the hypothesis that polarization of sensitized 5xxx Al alloys to large cathodic overpotentials causes crack arrest by setting up significantly alkaline crack tip conditions that promote corrosion-induced blunting.[4-5,34-35]

Specific conclusions include:

➢ The use of flexible esophageal microelectrodes allows a reliable method of crack tip pH sampling through consistently reproducible measurements regardless of the location of the external reference electrode.

➢ The application of a cathodic potential of −1.3 V_{SCE} halts sensitized AA5456-H116 CF da/dN when loading under low f at 0.1 Hz and leads to an alkaline crack tip environment with a pH of about 12.

➢ The crack tip pH of an actively growing CF crack in sensitized AA5456-H116 under freely corroding conditions is acidic compared to the bulk pH at a pH of between 2 and 4.

➢ The crack tip pH of corrosion fatigue cracks in AA5456-H116 under low f loading is similar to that of 7xxx Al alloys under SCC loading conditions.

ACKNOWLEDGMENTS

The authors would like to thank Dr. David Schrock for his previous work on AA5646, which led to this research focus. The authors would also like to thank Prof. Robert Kelly for the discussion on the crack tip pH probing technique he utilizes. Finally, useful discussions with Drs. Ramgopal Tholda and Gerald Frankel are gratefully acknowledged as they assisted in determining methods to increase peer confidence in our method. The preliminary research on AA7075 was funded through the National Science Foundation under grant number 1644972. The research on AA5456 was funded through the National Science Foundation under grant number 1943870. Any opinions, findings, conclusions, or recommendations expressed in this material are those of the authors and do not necessarily reflect the views of the National Science Foundation. The 5456 physical material was obtained through a prior Office of Naval Research grant N00014-16-1-2756 with Dr. Airan Perez as the Scientific Officer. Any opinions, findings, conclusions, or recommendations expressed in this material are those of the authors and do not necessarily reflect the views of the Office of Naval Research.

References

1. N.J.H. Holroyd, G.M. Scamans, *Corrosion* 72, 2 (2016): p. 136-143.
2. M.A. Wahid, A.N. Siddiquee, Z.A. Khan, "Aluminum Alloys in Marine Construction: Characteristics, Application, and Problems from a Fabrication Viewpoint," in *Marine Systems and Ocean Technology* (New York, NY: Springer, 2020), p. 70-80.
3. R. Niederberger, J. Basil, G. Bedford, *Corrosion* 22 (1966): p. 68-73.
4. M.E. McMahon, J.R. Scully, J.T. Burns, *Corrosion* 75 (2019): p. 911-928.
5. Z.D. Harris, E.M. Dubas, D.J. Schrock, J.S. Locke, J.T. Burns, *Mater. Sci. Eng. A* 792 (2020): article id 139792.

6. D.J. Schrock, A.M. Akman, J.S. Locke, *Corrosion* 77 (2021): p. 287-297.
7. R.M. Bay, D.J. Schrock, A.M. Akman, L.G. Bland, R. Thodla, J.S. Locke, *Int. J. Fatigue* 124 (2019): p. 1-9.
8. M. Steiner, S. Agnew, *Scr. Mater.* 102 (2015): p. 55-58.
9. M. Steiner, S. Agnew, *Corrosion* 72, 2 (2016): p. 169-176.
10. E. Bumiller, "Intergranular Corrosion in AA5XXX Aluminum Alloys with Discontinuous Precipitation at the Grain Boundaries" (Ph.D. diss., University of Virginia, 2011).
11. A.J. Davenport, Y. Yuan, R. Ambat, B.J. Connolly, M. Strangwood, A. Afseth, G.M. Scamans, *Mater. Sci. Forum* 519–521 (2006): p. 641-646.
12. S. Jain, M. Lim, J. Hudson, J. Scully, *Corros. Sci.* 59 (2012): p. 136-147.
13. L. Kramer, M. Phillippi, W. Tack, C. Wong, *J. Mater. Eng. Perform.* 21 (2012): p. 1025-1029.
14. M. Lim, J. Scully, R. Kelly, *Corrosion* 69 (2013): p. 35-47.
15. M.L.C. Lim, R.G. Kelly, J.R. Scully, *Corrosion* 72, 2 (2016): p. 198-220.
16. M.L.C. Lim, R. Matthews, M. Oja, R. Tryon, R.G. Kelly, J.R. Scully, *Mater. Des.* 96 (2016): p. 131-142.
17. E. Dix Jr., W. Anderson, M.B. Shumaker, *Corrosion* 15 (1959): p. 19-26
18. W. Gao, Y. Gu, L. Chen, H. Liang, D. Wang, M. Seifi, J.J. Lewandowski, *J. Mater. Res. Technol.* 25 (2023): p. 681-697.
19. W. Gao, D. Wang, M. Seifi, J.J. Lewandowski, *Mater. Sci. Eng. A* 740 (2019): p. 34-48.
20. R. Jones, D. Baer, M. Danielson, J. Vetrano, *Metall. Mater. Trans. A* 32 (2001): p. 1699-1711.
21. R.H. Jones, J.S. Vetrano, C.F. Windisch, *Corrosion* 60, 12 (2004): p. 1144-1154.
22. M. McMahon, P. Steiner, A. Lass, J. Burns, *Corrosion* 73 (2017): p. 713-723.
23. M.E. McMahon, P.J. Steiner, A.B. Lass, J.T. Burns, *Corrosion* 73 (2017): p. 347-361.
24. J. Searles, P. Gouma, R. Buchheit, *Metall. Mater. Trans. A* 32 (2001): p. 2859-2867.
25. M. Seifi, I. Ghamarian, P. Samimi, P. Collins, N. Holroyd, J. Lewandowski, *Corros. Sci.* 138 (2018): p. 219-241.
26. N. Kumar, G.P. Chaudhari, *Eng. Fail. Anal.* 156 (2024): p. 107782.
27. C.B. Crane, R.P. Gangloff, *Corrosion* 72, 2 (2016): p. 221-241.
28. J. Gunson, "Effect of Sensitisation on the Corrosion Fatigue Properties of AA5456-H116" (Master's thesis, University of Birmingham, 2011).
29. R.L. Holtz, P.S. Pao, R.A. Bayles, T.M. Longazel, R. Goswami, "Corrosion Fatigue of Al 5083-H131 Sensitized at 70, 100, and 175 C Relation to Microstructure and Degree of Sensitization," in DoD Corrosion Conference (Houston, TX: NACE/DoD, 2011).
30. R.L. Holtz, P.S. Pao, R.A. Bayles, T.M. Longazel, R. Goswami, *Metall. Mater. Trans. A* 43 (2012): p. 2839-2849.
31. M. Seifi, P. Samimi, I. Ghamarian, P.C. Collins, J.J. Lewandowski, *Philos. Mag. Lett.* 95 (2015): p. 526-533.
32. D.J. Schrock, J.S. Locke, *Corrosion* 76 (2020): p. 63-70.
33. ASTM B G67-04, "Standard Test Method for Determining the Susceptibility to Intergranular Corrosion of 5XXX Series Aluminum Alloys by Mass Loss After Exposure to Nitric Acid (NAMLT Test)" (West Conshohocken, PA: ASTM International, 2004).
34. M.E. McMahon, Z.D. Harris, J.R. Scully, J.T. Burns, *Mater. Sci. Eng. A* 767 (2019): article id 138399.
35. D.J. Schrock, "The Effects of Loading Frequency, Sensitization Level, and Electrochemical Potential on Corrosion Fatigue Kinetics of Aluminum-Magnesium Alloys" (Ph.D. diss., The Ohio State University, 2020).
36. J.K. Donald, J. Ruschau, "Direct Current Potential Difference Fatigue Crack Growth Measurement Techniques," in *Fatigue Crack Measurement: Techniques and Applications*, eds. K.J. Marsh, R.A. Smith, R.O. Ritchie (West Midland, United Kingdom: EMAS, 1991), p. 11-38.
37. ASTM E647, "Standard Test Method for Measurement of Fatigue Crack Growth Rates" (West Conshohocken, PA: ASTM International, 2015).
38. K.R. Cooper, R.G. Kelly, *Corros. Sci.* 49 (2007): p. 2636-2662.
39. K.R. Cooper, "Chemistry and Electrochemistry of Environment-Assisted Cracking of Al-Zn-Mg-Cu Alloy" (Ph.D. diss., University of Virginia, 2001).
40. K.R. Cooper, R.G. Kelly, *J. Chromatogr. A* (1999): p. 381-389.
41. A. Turnbull, *Mater. Sci. Technol.* 1, 9 (1985): p. 700-710.
42. T.H. Nguyen, B.F. Brown, R.T. Foley, *Corrosion* 38 (1982): p. 319-326.